A Versatile Cathodic "Signal-on" Photoelectrochemical Platform Based on a Dual-Signal Amplification Strategy

Ying Li, Fengting Chen, Zhenzhu Luan, Xiaoru Zhang

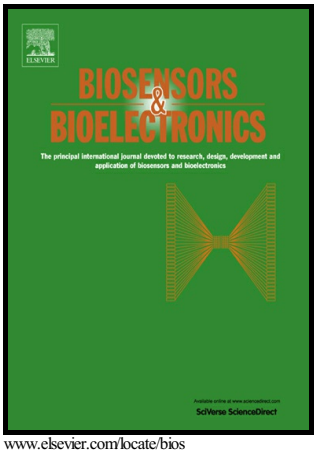

www.elsevier.com/locate/bios

PII: S0956-5663(18)30578-5
DOI: https://doi.org/10.1016/j.bios.2018.07.068
Reference: BIOS10657

To appear in: *Biosensors and Bioelectronic*

Received date: 4 June 2018
Revised date: 27 July 2018
Accepted date: 30 July 2018

Cite this article as: Ying Li, Fengting Chen, Zhenzhu Luan and Xiaoru Zhang, A Versatile Cathodic "Signal-on" Photoelectrochemical Platform Based on a Dual-Signal Amplification Strategy, *Biosensors and Bioelectronic,* https://doi.org/10.1016/j.bios.2018.07.068

A Versatile Cathodic "Signal-on" Photoelectrochemical Platform Based on a Dual-Signal Amplification Strategy

Ying Li[a], Fengting Chen[a], Zhenzhu Luan[b], Xiaoru Zhang[b,c,*]

[a]*Key Laboratory of Sensor Analysis of Tumor Marker, Ministry of Education, College of Chemistry and Molecular Engineering, Qingdao University of Scienceand Technology, Qingdao 266042, PR China.*

[b]*Shandong Key Laboratory of Biochemical Analysis, College of Chemistry and Molecular Engineering, Qingdao University of Scienceand Technology, Qingdao 266042, PR China.*

[c]*Key Laboratory of Analytical Chemistry for Life Science in Universities of Shandong, College of Chemistry and Molecular Engineering, Qingdao University of Scienceand Technology, Qingdao 266042, PR China. E-mail address: zhangxr7407@126.com*

ABSTRACT: Novel cathodic photoelectrochemical (PEC) aptasensors for sensitive and selective determination of thrombin and Pb^{2+} were developed based on a new dual-signal amplification strategy. The presence of gold nanoparticles (AuNPs) could quench the PEC signal of bismuth oxyiodide (BiOI). At the same time, the redox moiety G-quadruplex/hemin or ferrocene (Fc) was found to enhance the PEC signal of BiOI. So, in the presence of thrombin or Pb^{2+}, the interaction between target and the aptamer resulted in the releasement of the AuNPs, as well as shorter distance between the redox moiety and the electrode surface. Hence dual-enhanced cathodic PEC biosensor strategy was realized. Under the optimized conditions, the detection limits of thrombin and Pb^{2+} were 17.3 fM and 3.16 pM, respectively with good selectivity. At the same time, the PEC performance of redox moiety G-quadruplex/hemin and Fc was compared.

***Keywords*:** photoelectrochemistry; cathodic photocurrent; thrombin; Pb^{2+}

1. Introduction

Photoelectrochemical (PEC) is a recently emerged yet vibrantly developing analytical method for biological sensing (Li et al., 2018a). Benefiting from total separation between excitation source (light) and detection signal (current), PEC detection has received substantial attention owing to its potentially high sensitivity and low background signal (Li et al., 2018b). Besides, PEC has also some other advantages, for example the PEC instrument is simple, portable, and inexpensive compared with traditional optical assays (Ma et al., 2018). To date, many different kinds of target analytes such as proteins, metal ions, cells, microRNA and DNA, have been successfully detected by PEC biosensor. Of course, the properties of photoactive material play a major role in the analytical performance of the PEC sensors. According to the types of charge carrier, inorganic semiconductor material involved in PEC detection could be divided into two groups: n-type and p-type (Hisatomi et al., 2014). Up to now, previous works mainly rely on the photoanodes of n-type semiconductors such as CdSe (Yan et al., 2014), CdS (Zheng et al., 2015; Zhao et al., 2012c; Zhao et al., 2012b; Zhao et al., 2012a), ZnO and TiO_2 (Zhao et al., 2013; Zhao et al., 2012d; Kang et al., 2010), which can efficiently convert visible light or UV irradiation to anodic current. However, the applications of these n-type semiconductors can be interfered by the competitive reactions of the reductive ingredient in the real samples such as, H_2O_2 (An et al., 2010), dopamine (Hao et al., 2012), ascorbic acid (Zhao et al., 2012a; Kang et al., 2010), thio compounds (Long et al., 2011; Tang et al., 2013) and nicotinamide adenine dinucleotide (Zhao et al., 2014), which is easily absorbed on the surface of electrode. Then the adsorbed reductive ingredient will compete with a sacrificial electron donor in the buffer and result in false positive photocurrent signal (Wang et al., 2014; Wang et al., 2015b). This defect highly restricts the application of n-type semiconductors in the complex detection system (Wang et al., 2015; Wang et al., 2015a).

As for p-type semiconductors based photocathode sensor, which need electron acceptor rather than electron donor to produce cathodic photocurrent, oxygen is the commonly used electron acceptor. In this process, electron firstly jumps from electrode to the valence band (VB) of photocathode material. And then, electron jumps from VB to the conduction band (CB) of photocathode material. Finally, electron jumps to electron acceptor-oxygen. Thus, the adsorbed reductive ingredient in the complex detection solution can not interfere with the cathodic photocurrent. Since holes are used as carriers for electron acceptor of photocathode sensor, the

photocurrent response is lower than that of photoanode sensor (Zhao et al., 2012a; Kong et al., 2013; Cheng et al., 2012). Owing to the small band gap and strong absorption in the visible light region, p-type semiconductor BiOI has been widely studied in the field of solar cell (Zhao et al., 2009), photocatalysis (Hu et al., 2018; Zhou et al., 2018) and photoelectronical biosensor. Using BiOI nanoflakes, Gong et al. have constructed a selective and sensitive biosensor to detect organophosphate pesticides (Gong et al., 2012) and Zhou et al. have fabricated a PEC biosensor to detect DNA methyltransferase activity (Zhou et al., 2014).

Here, we reported a novel cathodic "signal-on" photoelectrochemical biosensor based on a dual-signal amplification strategy. G-quadruplex/ hemin or Fc was reported to enhance the cathodic photocurrent of BiOI for the first time. This may be explained that G-quadruplex/ hemin or Fc can accept the electrons from the BiOI nanoplates and mediate the catalytic reduction of dissolved oxygen, which lead to the improvement of charge separation and the increase of cathodic photocurrent (Wang et al., 2015a; Fan et al., 2016). While, the AuNPs could quench the PEC signal of BiOI due to the electron transfer between AuNPs and BiOI nanoplates (Zhou et al., 2011; Wang et al., 2011). Using the dual-enhanced strategy, thrombin and Pb^{2+} can be detected sensitively and selectively. At the same time, the cathodic photocurrent generation of the BiOI nanoplates and electron transfer between BiOI and G-quadruplex/hemin or Fc were also investigated carefully.

2. EXPERIMENTAL SECTION

2.1 Materials and reagents

ITO electrodes (coating 30 ± 5 nm, sheet resistance ≤ 10 Ω/square) were obtained from Shenzhen CSG Display Technology Co., Ltd. Bismuth nitrate ($Bi(NO_3)_3{\cdot}5H_2O$) was obtained from Sahn Chemical Technology Co., Ltd. (Shanghai, China). Chitosan (CHIT) (degree of deacetylation >95.0%) was provided by Aladdin Reagent Co., Ltd. (Shanghai, China). Hemin was obtained from Alfa Aesar. Thrombin (TB), 1-(3-dimethylamino-propyl)- 3-ethylcarbodiimide hydrochloride (EDC), N-Hydroxysuccinimide (NHS) were ordered from Sigma-Aldrich. All the chemicals of highest purity grade were used without further purification. High purity water prepared by a Milli-Q water purification system with an electrical resistance of 18.2 MΩ was used throughout experiment. DNA oligonucleotides were synthesized by Sangon Biotech Co., Ltd. (Shanghai, China) with the following sequences:

Hemin aptamer DNA_1: 5'COOH(CH_2)-TTTTTTTTTTTTCCAACCACACCAACCAAGGG TTGGGCGGGATGGGTT-3';

Thrombin aptamer DNA_2: 5'-GGTTGGTGTGGTTGGTTTTTT-SH3';

Fc/DNA_3:5'COOH(CH_2)-TTTTTTTTTTTTCATCTCTTCTCCGAGCCGGTCGAAATAGTGAG T-Fc3';

Pb^{2+} aptamer DNA_4: 5'-ACTCACTATrAGGAAGAGATGTTTTTT-SH3'

2.2 Instruments.

The photocurrent and electrochemical impedance spectroscopy (EIS) were measured on an electrochemical work-station (Zahner, Zennium, Germany). An ITO electrode, a Pt wire and a saturated Ag/AgCl were employed as the working, counter and reference electrode, respectively. Light excitation of 460 nm was switched every 20 s. The absorption spectra of BiOI nanoplates were obtained on a Cary 50 UV/vis-NIR spectrophot-ometer (Varian). X-ray diffraction (XRD) patterns were obtained from a Philips X'pert Pro X-ray diffractometer (Brook AXS, Germany) with Cu Kα radiation. Field-emission scanning electron microscopy (FE-SEM) was carried out on a JEM-7500F scanning electron microscope (JEOL Ltd., Japan).

2.3 Synthesis of BiOI nanoplates and modification of ITO electrode.

BiOI nanoplates were synthesized according to previous literature method with a little modification (Yan et al., 2015). Typically, 30 mL of 0.1M $Bi(NO_3)_3 \cdot 5H_2O$ in ethylene glycol was added dropwisely into 30 mL of 0.1M KI dissolved in ethylene glycol under vigorous stirring. After stirring at room temperature for 1 h, an orange-red solution was obtained. Then, the solution was transferred into a Teflon-lined autoclave and heated at 160 ℃ for 12 h. The as-obtained precipitates were washed three times with ethanol and deionized water and then dried at 60 ℃ for 4 h to give powder products.

Prior to modification, the ITO slices were ultrasonically cleaned in acetone, 2 M NaOH and deionized water for 20 min in order, followed by being dried with nitrogen gas. 5 mg BiOI powder was ultrasonically dispersed in 5 mL deionized water containing 0.035% CHIT and 0.5% acetic acid for about 2 h to give homogeneous suspension. Then 25 μL of 1.0 $mg \cdot mL^{-1}$ suspension was dropped onto a clean ITO glass. After drying at 60 ℃, the electrode was rinsed with deionized water for several times giving ITO/BiOI/CHIT.

Synthesis of Au nanoparticles and modification of AuNPs with thrombin or Pb^{2+} aptamer probe (DNA_2 or DNA_4) were described in the supporting information.

2.4 Detection of thrombin.

Hemin aptamer DNA_1 was modified on ITO/BiOI/CHIT electrode surface through classic EDC and NHS coupling reactions. First, 10 μL of 1.0×10^{-5} M hemin aptamer DNA_1 was added to 90 μL PBS consisting of 0.4173 M EDC and 0.3476 M NHS for 1 h at room temperature to activate COOH groups. Then 25 μL mixture was dropped onto the electrode surface and incubated at 4 ℃ for 12 h under a moisture atmosphere. Subsequently, 25 μL of 1.0 μM hemin was spread onto the hemin aptamer DNA_1 immobilized electrodes and incubated at 37 ℃ for 50 min. Finally, 25 μL of AuNPs modified DNA_2 (synthesized in supporting information) was spread onto the electrode and hybridized with hemin-DNA_1 at 37 ℃ for 2 h. The electrode was washed with 10 mM PBS (pH 7.4) for three times after each modification step. The photocurrent of the ITO/BiOI/CHIT/DNA_1-hemin/ AuNPs-DNA_2 electrode was measured in 0.1 M Na_2SO_4 at a bias potential of −0.1 V. After incubated with different concentrations of thrombin at 37 ℃ for 50 min and washed with the 10 mM PBS (pH 7.4), the photocurrent response of the fabricated sensor was recorded.

2.5 Detection of Pb^{2+}

Fc-modified DNA_3 was coupled with ITO/BiOI/CHIT electrode as described above with a little modification. First, 10 μL of 1.0×10^{-5} M Fc-modified DNA_3 was added to 90 μL PBS consisting of 0.3652 M EDC and 0.3041 M NHS at ambient temperature for 1 h to activate their COOH groups. Then 25 μL mixture was dropped onto the electrode surface and incubated at 4 ℃ for 12 h under a moisture atmosphere. Subsequently, 25 μL of AuNPs modified DNA_4 (synthesized in supporting information) was spread onto the electrodes at 37 ℃ for 2 h to hybridize with Fc-DNA_3. The electrode was washed with 10 mM PBS (pH 7.4) for three times after each modification step. The photocurrent of the ITO/BiOI/CHIT/DNA_3-Fc/AuNPs-DNA_4 electrode was detected in 0.1M Na_2SO_4 at a bias potential of −0.1 V. After incubated with different concentrations of Pb^{2+} at 37 ℃ for 2 h and washed with the PBS, the photocurrent of the fabricated sensor was recorded.

3. RESULTS AND DISCUSSION

3.1 Principle of PEC aptasensor for thrombin and Pb^{2+} detection.

On the basis of the photocurrent enhancement of BiOI nanoplates by hemin intercalated in the G-quadruplex and the photocurrent quenching effect of AuNP, G-quadruplex/hemin/AuNP hybrid system was assembled on BiOI nanoplates to construct a double signal-on biosensing platform for detecting thrombin. The detection principle was depicted in **Fig. 1A**. As cathodic photoelectrochemical materials, BiOI nanoplates conjugated with chitosan were coated on a clean ITO electrode. Then chitosan could provide amino- group for coupling with carboxylated hemin aptamer DNA_1. The hemin aptamer DNA_1 consisted two parts: domain **a** could form a G-quadruplex and domain **b** could hybridize with the AuNPs modified DNA_2. After the addition of hemin, domain **a** could form G-quadruplex/hemin hybrids on the surface of BiOI nanoplates. Thus a great enhancement for cathodic photocurrent was observed due to the photoinduced electron transfer (PET) from the CB of BiOI to G-quadruplex/hemin hybrids and then to dissolved oxygen. When AuNPs modified DNA_2 was introduced, a double-stranded DNA was formed due to the hybridization of DNA_2 with the domain **b** of DNA_1. Unlike flexible single-stranded DNA, such rigid double-stranded DNA structure kept G-quadruplex/ hemin hybrids relatively far from the electrode surface. So the electron transfer efficiency was reduced. Moreover, after hybridization, AuNPs were close to the electrode surface, interparticle energy-transfer from BiOI to AuNPs also led to the reduction of cathodic photocurrent. When target thrombin was added, the recognition between thrombin and DNA_2 modified on AuNPs led to the dissociation of AuNPs from electrode to the solution. At the same time, single-stranded DNA attached the G-quadruplex/ hemin was returned to the electrode surface, which could facilitate the electron transfer process. Based on the double enhanced PEC aptasensor, significant signal restore could be obtained.

During experiment, we found that although hemin could enhance photoelectrochemical signal greatly, its signal was unstable and there were always some differences between each measurement. This may be caused by the difficulty in the formation of G-quadruplex/ hemin hybrids. However, Fc enhancement for photocurrent signal was relatively stable. So, Fc instead of hemin was used to detect Pb^{2+}. The detection of Pb^{2+} utilizing the BiOI nanoplates-Fc hybrid was illustrated in Fig. 1B. Fc-modified DNA_3 was assembled on the electrode ITO/BiOI/CHIT through amido bond as described above. Once again, photocurrent was enhanced obviously due to the PET from the CB of BiOI nanoplates to Fc and then to dissolved oxygen. After addition of AuNPs modified DNA_2, similarly, photocurrent signal was reduced significantly due to the double

quenching effect of AuNPs and the relatively long distance of Fc to the electrode surface. However, in the presence of Pb^{2+}, which could cleave the AuNPs modified DNA_4 into two fragments, cathodic photocurrent was restored due to the dual-signal amplification effect as described above. Hence, a PEC biosensor for the detection of Pb^{2+} was fabricated.

Fig. 1

3.2 Characterization of materials

As shown in the X-ray diffraction (XRD) pattern (Fig. S1A in supporting information), BiOI nanoplates showed typical diffraction peaks located at 29°, 32°, 46°, 55° and 67°, corresponding to the (102), (110), (200), (212) and (220) diffraction planes of the standard tetragonal BiOI [JCPDS Card No. 73–2062]. This means the successful formation of the pure crystalline BiOI. At the same time, BiOI nanoplate exhibited an absorbance peak at ca. 553 nm (Fig. S1B in supporting information), indicating its suitability to be a photoactive material.

SEM was performed to confirm the successful assembly of BiOI and AuNPs on the electrode. Fig. 2A was a typical SEM image of BiOI-CHIT modified ITO electrode. The presence of sticky chitosan led to the layered structure on ITO electrode, which indicated the successful immobilization of the BiOI nanoplates on the ITO electrode. The stability of prepared BiOI-chitosan complex was good and could be used for at least 2-3 months. Fig. 2B and insert in Fig. 2B were a typical SEM image of ITO/ BiOI/ DNA_1-hemin electrode. When DNA and hemin were coupled on the ITO electrode, the aggregation degree was deepened. Once hybridization with AuNPs modified DNA_2, AuNPs were uniformly distributed on BiOI nanoplates (Fig. 2C and insert in Fig. 2C), indicating the well-behaved assembly process. SEM images of BiOI nanoplates assembled with Fc-modified DNA_3 and AuNPs modified DNA_4 showed identical images as described above (see Fig. S2A and Fig. S2B in supporting information).

Fig. 2

UV-vis and CD spectra were used to verify the formation of G-quadruplex/hemin conjugate (see Fig. S3 in supporting information for details) .

3.3 The mechanism for the cathodic photocurrent generation

The mechanism of photocurrent generation by BiOI nanoplates was illustrated in Fig. 3A. The CB and VB potentials of BiOI nanoplates were −1.15V and 0.55V respectively *vs* the normal

hydrogen electrode (NHE), (see Fig. S4 in supporting information for details). Firstly, ITO electrode donated an electron to VB of BiOI. As a p-type semiconductor, BiOI with a narrow band gap could be excited easily. Then the photogenerated electrons in the CB of BiOI were trapped by O_2 dissolved in 0.1M Na_2SO_4 electrolyte and generated a cathodic photocurrent. After introduction of G-quadruplex/hemin hybrids to the surface of BiOI nanoplates modified ITO electrode, enhanced cathodic photocurrent was observed (Fig. 4A). The reduction potential of the G-quadruplex/hemin hybrid was −0.178V vs NHE, which was the same as Fe^{III}/ Fe^{II}-protoporphyrin IX couple reported previously (Zhang et al., 2013). Thus, the potential gradient favored the electron transfer from the CB of BiOI (−1.15V vs NHE) to G-quadruplex/hemin hybrids (−0.178V vs NHE, see Fig. 3B). This process could inhibit the recombination of electron−hole pairs, resulting in the further improvement of the photocurrent response. Similarly, a reduction potential of Fc was estimated to be 0.17 V vs Ag/AgCl (i.e., 0.37 V vs NHE) (see Fig S5 in supporting information). So the electron transfer from the CB of the BiOI nanoplates (−1.15V vs NHE) to Fc (0.37 V vs NHE) was also favored (see Fig.3C).

Fig. 3

3.4 PEC response of sensor and electrochemical impedance analysis

To study the photocurrent influence for different assemble step, as well as the feasibility of the developed biosensor, the change of photocurrent during each fabrication step was investigated. As presented in Fig. 4, curve a or a' represented the photocathode of ITO/BiOI. When introducing of hemin aptamer DNA or Fc modified DNA enzyme on the surface of ITO/BiOI, the photocurrent intensity increased greatly due to the improved electron-transfer between BiOI and hemin or Fc (curve b or b'). After hybridization with AuNPs modified DNA, the photocurrent intensity decreased dramatically (curve c or c') due to the relatively long spacing distance from G-quadruplex/ hemin hybrids or Fc to the electrode and the photocurrent quenching effect of AuNPs. Finally, after addition of 8.75×10^{-9} M thrombin or 1.0×10^{-6} M Pb^{2+}, the recognition of thrombin with aptamer or the incision of DNAzyme led to the increase of photocurrent again due to the removal of AuNPs and the distance restoration of G-quadruplex/ hemin hybrids or Fc. Thus, the developed PEC biosensor could be used for the detection of thrombin or Pb^{2+}.

Fig. 4

The interface property of the electrode for each fabrication step was also characterized by electrochemical impedance spectroscopy (EIS). The increase in the diameter of Nyquist plots semicircle reflects the increase in the electron-transfer resistance (R_{et}). As shown in Fig S6 of supporting information, the bare ITO electrode exhibited a small semicircle (curve a or a'). When BiOI and CHIT were coated on the surface of ITO, the R_{et} value increased obviously (curve b or b'), owning to the poor conductivity of the semiconductors. The assembly of the hemin aptamer-hemin hybrids or Fc modified DNAzyme further suppressed the charge transfer due to the electrostatic repulsion between the negatively charged DNA and $Fe(CN)_6^{3-/4-}$, as well as the steric hindrance effect (curve c or c'). Upon hybridization with the AuNPs modified DNA, the R_{et} value was increased dramatically (curve d or d'). After incubation with thrombin or Pb^{2+}, the R_{et} value decreased (curve e or e'), indicating the departure of AuNPs modified DNA caused by the recognition between thrombin and its aptamer or the incision of DNAzyme. The results further proved the successful assembly process.

3.5 The linear relationship of thrombin and Pb^{2+} detection.

Using this double signal-on biosensing platform thrombin and Pb^{2+} were quantitatively determined. ITO/BiOI/hemin-DNA_1/AuNPs-DNA_2 system was applied to the detection of thrombin. Under optimum conditions (discussed in Fig. S7 of supporting information), the photocurrent response increased with increasing concentration of thrombin (see Fig. 5A). A good linear correlation between the change of photocurrent and the thrombin concentration ranging from 8.75×10^{-14} to 8.75×10^{-9} M was obtained (see Fig. 5B). The linear regression equation was expressed as $\Delta PI\ (nA)=159.67\lg C_{TB}\ (M)+2066.54$, with a correlation coefficient (R^2) of 0.9921. The detection limit for thrombin was found to be 17.3 fM, and the relative standard deviation (RSD) was 6.1%. The sensitivity for thrombin of this method is better than most methods developed previously (Table S1).

Similarly, the developed ITO/BiOI/Fc-DNA_3/AuNPs-DNA_4 system was applied to the quantitative determination of Pb^{2+}. The detection conditions were optimized in Fig. S8 of supporting information. As shown in Fig. 5C, with the increasing Pb^{2+} concentration, the photocurrent increased accordingly. The photocurrent intensity was logarithmically related to Pb^{2+} concentrations across the range from 5.0×10^{-12} M to 1.0×10^{-6} M (see Fig. 5D). The linear regression equation was expressed as $\Delta PI\ (nA)= 75.48\ \lg C_{Pb^{2+}}\ (M) + 892.93$, with a correlation

coefficient (R^2) of 0.9982. The detection limit for Pb^{2+} was found to be 3.16 pM, and the relative standard deviation (RSD) was 4.1%. Compared with previously reported methods for Pb^{2+} determination (Table S2), the sensitivity of proposed PEC aptamer sensor is good.

However, the signal change for ITO/BiOI/hemin-DNA_1/AuNPs-DNA_2 system was higher than that of ITO/BiOI/Fc-DNA_3/AuNPs-DNA_4 system, while the signal stability of ITO/BiOI/ Fc-DNA_3/AuNPs-DNA_4 system was much better. Considering the practical application, the later system using Fc as a probe is more valuable.

Fig. 5

3.6 Selectivity of the PEC biosensor.

Control experiments were carried out to test the selectivity of the developed photoelectrochemical aptasensor. From the results shown in Fig. 6A, the photocurrent responses to other potential interfering agents, including bovine serum albumin (BSA), hemoglobin (Hb) and lysozyme (Lyso) were much lower than that of thrombin (TB). Meanwhile, the mixture of protein did not show obvious interference in the determination of thrombin, confirming the specific interaction between aptamer and thrombin. The selectivity of ITO/BiOI/Fc-DNA_3/AuNPs-DNA_4 system for Pb^{2+} was investigated in Fig. 6B. The photocurrent responses to 100 times Mn^{2+}, Mg^{2+}, Ca^{2+}, Cu^{2+}, K^+, Fe^{3+}, Na^+, Hg^{2+} and their mixture were also recorded. The results showed that all these metal ions did not interfere with the determination of Pb^{2+}, demonstrating the specific recognition ability for these dual-signal amplification biosensors.

Fig. 6

3.7 Practical application in complex sample

Standard addition method was used to test the practical applicability of the proposed method in complex samples. Firstly, 10% diluted human serum samples spiked with different concentrations of thrombin were measured using ITO/BiOI/hemin-DNA_1/AuNPs-DNA_2 system. The recoveries obtained by these added thrombin were found to vary from 96.5% to 102.7%(see Table S3 in supporting information). Then tap water samples spiked with different concentrations of Pb^{2+} were tested using ITO/BiOI/Fc-DNA_3/AuNPs-DNA_4 system. The recoveries were found to vary from 96.8% to 104.2% (see Table S4 in supporting information). These results suggested that the developed dual-signal amplification PEC biosensors had good potential for practical sensing in complex samples.

4. CONCLUSIONS

In summary, two novel double signal-on cathodic PEC biosensor platforms were developed termed as ITO/BiOI/hemin-DNA_1/AuNPs-DNA_2 system and ITO/BiOI/Fc-DNA_3/AuNPs-DNA_4 system. Hemin-DNA1 and Fc was found to enhance the cathodic photocurrent of BiOI nanoplates for the first time. After introducing AuNPs through the hybridization of DNA, photocurrent signal was reduced significantly due to the double quenching effect of AuNPs and the relatively long distance of hemine or Fc to the electrode surface. The presence of target thrombin or Pb^{2+} led to the departure of AuNPs and the conformation recovery for hemin or Fc on the electrode. Thus significant enhancement of photocurrent was observed. Using this dual-enhanced strategy, thrombin and Pb^{2+} could be detected sensitively with high selectivity. Compared these two biosensors, the signal change for ITO/BiOI/hemin-DNA_1/AuNPs-DNA_2 system is higher than that of ITO/BiOI/Fc-DNA_3/AuNPs-DNA_4 system. However, the signal stability of ITO/BiOI/Fc-DNA_3 /AuNPs-DNA_4 system was much better. Considering the practical application, we think the later system using Fc as probe is more valuable.

Acknowledgements

This work has been financially supported by the National Natural Science Foundation of China (No.: 21775080), Key Research and Development project of Shandong Province (Nos. 2017GSF221004, 2018GSF121010).

REFERENCES

An, Y. R., Tang, L. L., Jiang, X. L., Chen, H., Yang, M. C., Jin, L.T., Zhang, S. P., Wang, C. G., Zhang, W., 2010. Chem. Eur. J. 16, 14439−14446.

Cheng, L. Y., Zhou, J., Zou, Q., Long, Y. T., Tian, H., 2012. RSC Adv. 2, 4623−4626.

Fan, G. C., Shi, X. M., Zhang, J. R., Zhu, J. J., 2016. Anal. Chem. 88, 10352−10356.

Gong, J., Wang, X., Li, X., Wang, K., 2012. Biosens. Bioelectron. 38, 43−49.

Hao, Q., Wang, P., Ma, X. Y., Su, M. Q., Lei, J. P., Ju, H. X., 2012. Electrochem. Commun. 21, 39−41.

Hisatomi, T., Kubota, J., Domen, K., 2014. Chem. Soc. Rev. 43, 7520−7535.

Hu, L. L., He, H. J. W., Xia, D. H., Huang, Y. J., Xu, J. R., Li, H. Y., He, C., Yang, W. J., Shu, D., Wang, P. K., 2018. ACS Appl. Mater. Interfaces. 10, 18693-18708.

Kang, Q., Yang, L. X., Chen, Y. F., Luo, S. L., Wen, L. F., Cai, Q. Y., Yao, S. Z., 2010. Anal. Chem. 82, 9749−9754.

Kong, C., Zhang, G., Li, Y., Li, D. W., Long, Y. T., 2013. RSC Adv. 3, 3503−3507.

Li, M. J., Xiong, C., Zheng, Y. N., Liang, W. B., Yuan, R., Chai, Y. Q., 2018a. Anal. Chem. 90, 8211-8216.

Li, L., Wang, T., Zhang, Y., Xu, C. X., Zhang, L. N., Cheng, X., Liu, H., Chen, X. D., Yu, J. H., 2018b. ACS Appl. Mater. Interfaces. 10, 14594-14601.

Ma, H. M., Fan, Q., Fan, B. B., Zhang, Y., Fan, D. W., Wu, D., Wei, Q., 2018. Langmuir. 34, 7744-7750.

Ma, Z. Y., Ruan, Y. F., Zhang, N., Zhao, W. W., Xu, J. J., Chen, H. Y., 2015. Chem.Commun. 51, 8381--8384.

Tang, J., Kong, B., Wang, Y. C., Xu, M., Wang, Y. L., Wu, H., Zheng, G. F., 2013. NanoLett. 13, 5350−5354.

Wang, G. L., Liu, K. L., Dong, Y. M., Wu, X. M., Li, Z. J., Zhang, C., 2014. Biosens. Bioelectron. 62, 66−72.

Wang, G. L., Liu, K. L., Shu, J. X., Gu, T. T., Wu, X. M., Dong, Y. M., Li, Z. J., 2015a. Biosens. Bioelectron. 69, 106−112.

Wang, G. L., Shu, J. X., Dong, Y. M., Wu, X. M., Zhao, W. W., Xu, J. J., Chen, H. Y., 2015b. Anal. Chem. 87, 2892−2900.

Wang, J., Shan, Y., Zhao, W. W., Xu, J. J., Chen, H. Y., 2011. Anal. Chem. 83, 4004−4011.

Yan, k., Liu, Y., Yang, Y. H., Zhang, J. D., 2015. Anal. Chem. 87, 12215−12220.

Yan, K., Wang, R., Zhang, J. D., 2014. Biosens. Bioelectron. 53, 301-304.

Zang, Y., Lei, J. P., Hao, Q., Ju, H. X., 2016. Biosens. Bioelectron. 77, 557-564.

Zhang, L. B., Zhu, J. B., Guo, S. J., Li, T., Li, J., Wang, E. K., 2013. J. Am. Chem. Soc. 135, 2403−2406.

Zhao, K., Zhang, X., Zhang, L., 2009. Electrochem. Commun. 11, 612−615.

Zhao, W. W., Dong, X. Y., Wang, J., Kong, F. Y., Xu, J. J., Chen, H. Y., 2012a. Chem. Commun. 48, 5253−5255.

Zhao, W. W., Liu, Z., Shan, S., Zhang, W. W., Wang, J., Ma, Z.Y., Xu, J. J., Chen, H. Y., 2014. Sci. Rep. 4, 4426−4431.

Zhao, W. W., Ma, Z. Y., Xu, J. J., Chen, H. Y., 2013. Anal. Chem. 85, 8503−8506.

Zhao, W. W., Ma, Z. Y., Yu, P. P., Dong, X. Y., Xu, J. J., Chen, H. Y., 2012b. Anal. Chem. 84, 917−923.

Zhao, W. W., Yu, P. P., Shan, Y., Xu, J. J., Chen, H. Y., 2012c. Anal. Chem. 84, 5892−5897.

Zhao, W. W., Zhang, L., Xu, J. J., Chen, H. Y., 2012d. Chem. Commun. 48, 9456−9458.

Zhou, H., Liu, J., Xu, J. J., Chen, H.Y., 2011. Anal. Chem. 83, 8320−8328.

Zhou, X. J., Shao, C. L., Yang, S., Li, X. W., Guo, X. H., Wang, X. X., Li, X. H., Liu, Y. C., 2018. ACS Sustainable Chem. Eng. 6, 2316-2323.

Zhou, Y., Xu, Z., Wang, M., Sun, B., Yin, H., Ai, S., 2014. Biosens. Bioelectron. 53, 263−267.

Figure captions

Fig. 1 Schematic Illustration of the dual-enhancement aptasensor for **(A)** TB detection; (B) Pb^{2+} detection.

Fig. 2 SEM images of (A) BiOI-CHIT modified ITO electrode (A) ; (B) ITO/BiOI-CHIT modified with hemin aptamer DNA_1 and hemin; (C) Electrode (B) hybridized with AuNPs modified DNA_2.

Fig. 3 (A) Mechanism for the cathodic photocurrent generation of the BiOI nanoplatesand; (B) Reduction potential of Hemin/G-Quadruplex conjugate and the energy levels of BiOI nanoplates; (C) Reduction potential of Fc and the energy levels of BiOI nanoplates.

Fig. 4 (A) Photocurrent responses in 0.1 M Na_2SO_4 at a bias potential of −0.1 V for (a, a') ITO/ BiOI; (b, b') ITO/BiOI/hemin or Fc-DNA; (c, c') ITO/BiOI/hemin or Fc-DNA/AuNPs-DNA; (d, d') ITO/BiOI/hemin or Fc-DNA/AuNPs-DNA incubated with 8.75×10^{-9} M thrombin or 1.0×10^{-6} M Pb^{2+}.

Fig. 5 (A) Photocurrent responses of the fabricated sensor incubated with different concentrations of thrombin: (from a to k 8.75×10^{-9}, 4.38×10^{-9}, 8.75×10^{-10}, 4.38×10^{-10}, 8.75×10^{-11}, 4.38×10^{-11}, 8.75×10^{-12}, 4.38×10^{-12}, 8.75×10^{-13}, 4.38×10^{-13}, 8.75×10^{-14} M). **(B)** Calibration curve for thrombin detection (C) Photocurrent responses of the fabricated sensor incubated with different concentrations of Pb^{2+}: (from a to l 1.0×10^{-6}, 5.0×10^{-7}, 1.0×10^{-7}, 5.0×10^{-8}, 1.0×10^{-8}, 5.0×10^{-9},

1.0×10^{-9}, 5.0×10^{-10}, 1.0×10^{-10}, 5.0×10^{-11}, 1.0×10^{-11}, 5.0×10^{-12} M**). (D)** Calibration curve for Pb^{2+} on the PEC sensor. Error bars were derived from the standard deviation of three measurements.

Fig. 6 Selectivity of the PEC aptasensor incubated (A) with TB, BSA, Hb, Lyso and the mixed sample. The concentrations of BSA, Hb, Lyso were 8.75×10^{-8} M, the concentrations of TB were 8.75×10^{-9} M; (B) Different metal ions (Pb^{2+}, Mn^{2+}, Mg^{2+}, Ca^{2+}, Cu^{2+}, K^{+}, Fe^{3+}, Na^{+}, Hg^{2+}, Fe^{2+}, Ni^{2+}, Co^{2+}, Cr^{3+}, Cr^{6+}), and the mixed metal ions sample. The concentration is 1.0×10^{-7} M for Pb^{2+}, and 1.0×10^{-5} M for other metal ions. The error bars show the standard deviation of three replicate determinations.

Highlights:

(1) G-quadruplex/hemin and ferrocene were found to enhance the cathodic photocurrent of BiOI for the first time.

(2) Cathodic “signal-on” photoelectrochemical biosensors were developed based on the dual-signal amplification strategy.

(3) The developed versatile platform can be used for the detection of thrombin and Pb^{2+}.

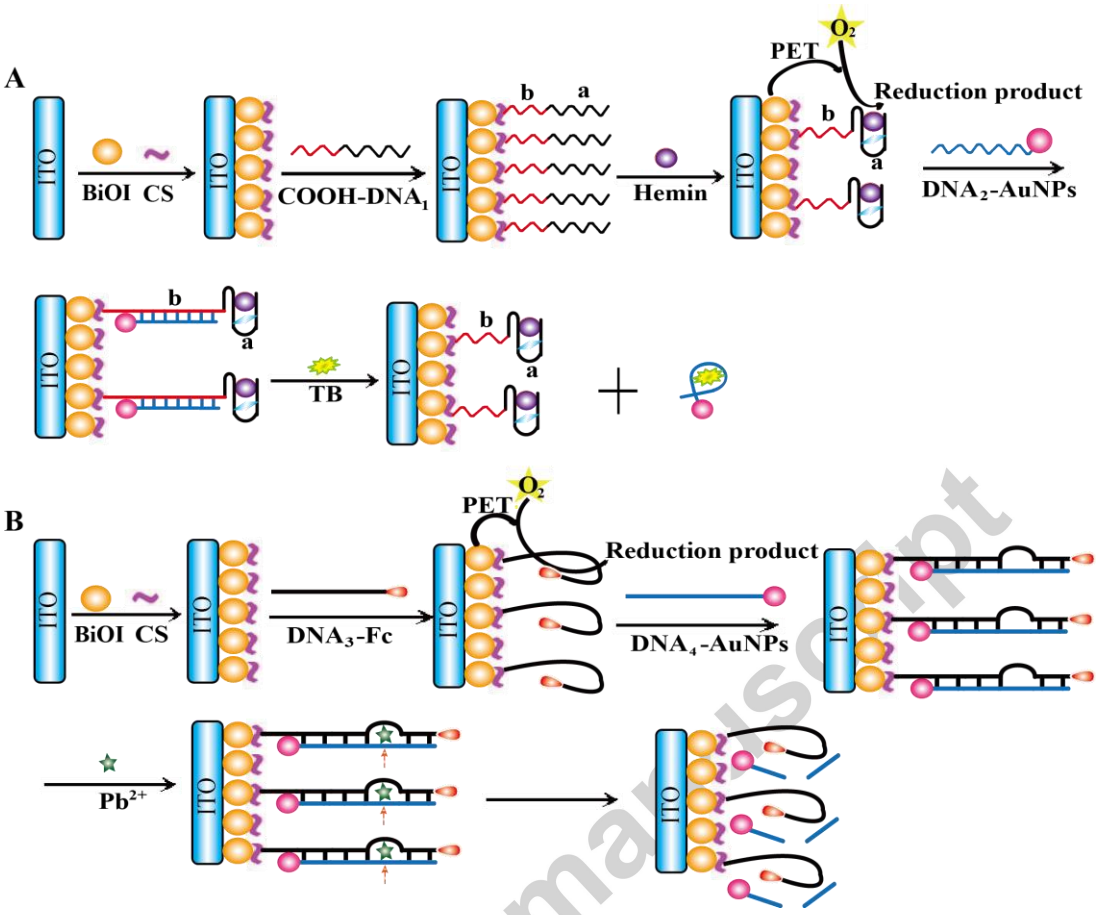

Fig. 1

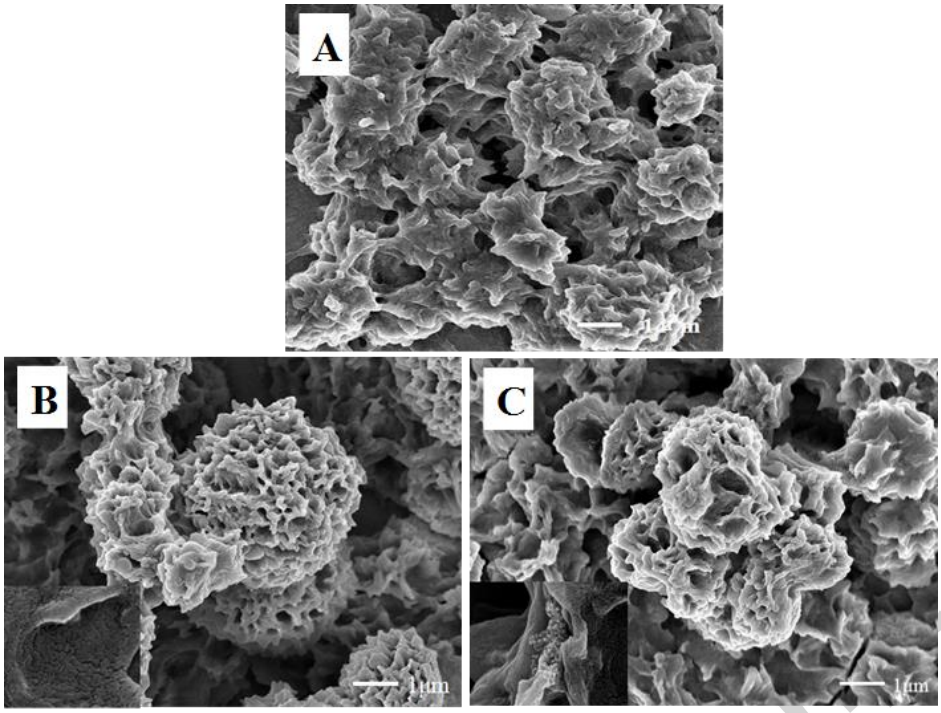

Fig. 2

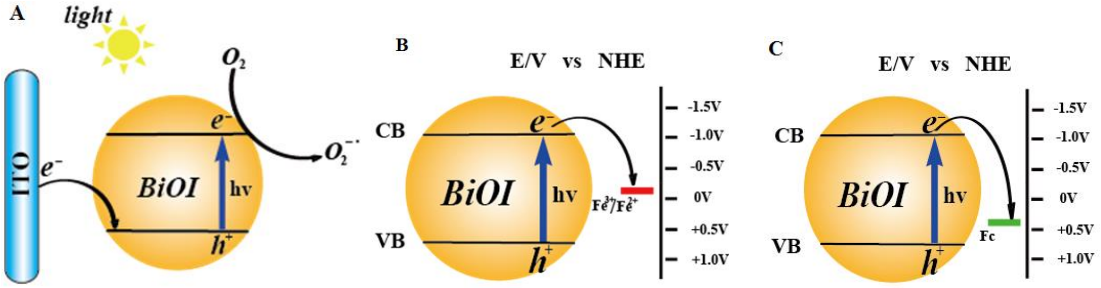

Fig. 3

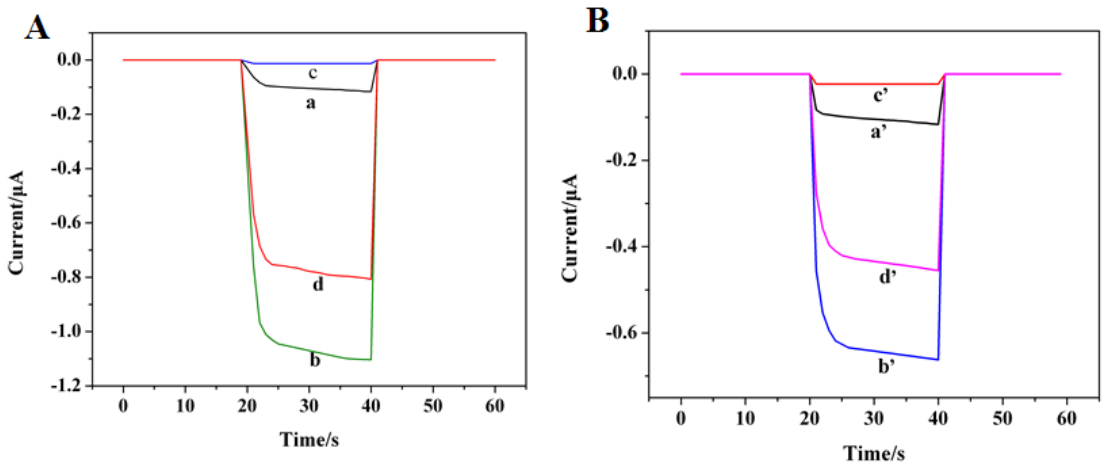

Fig. 4

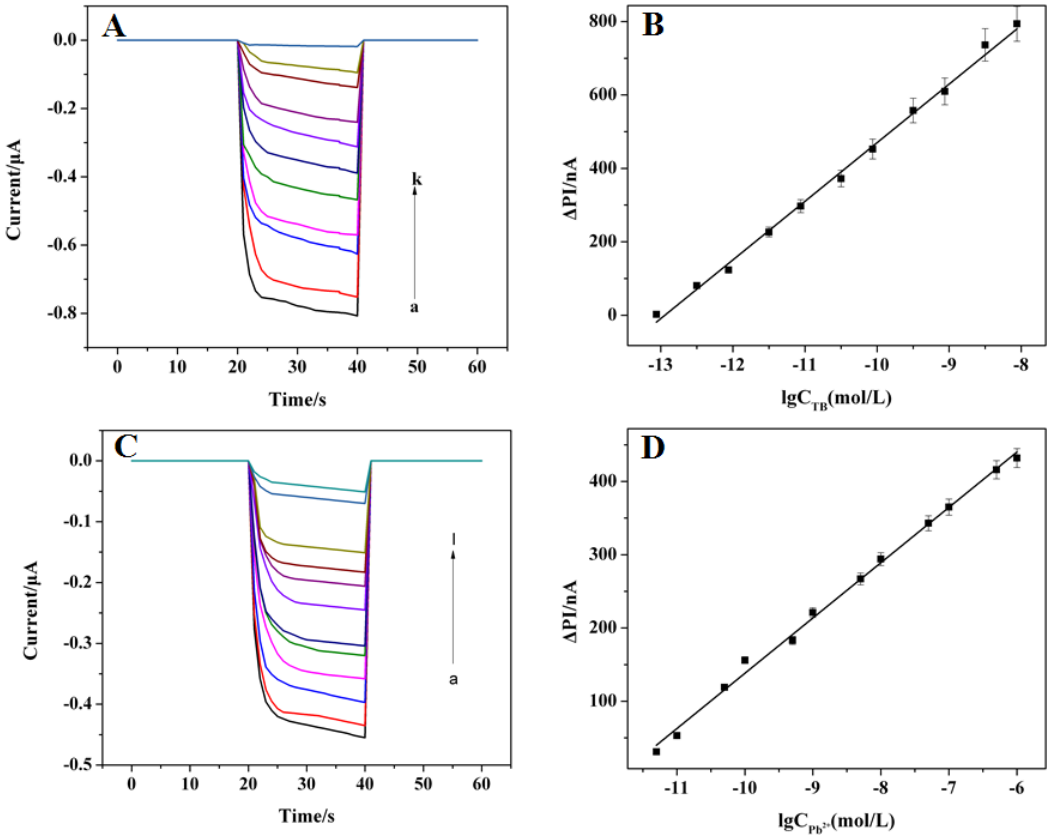

Fig. 5

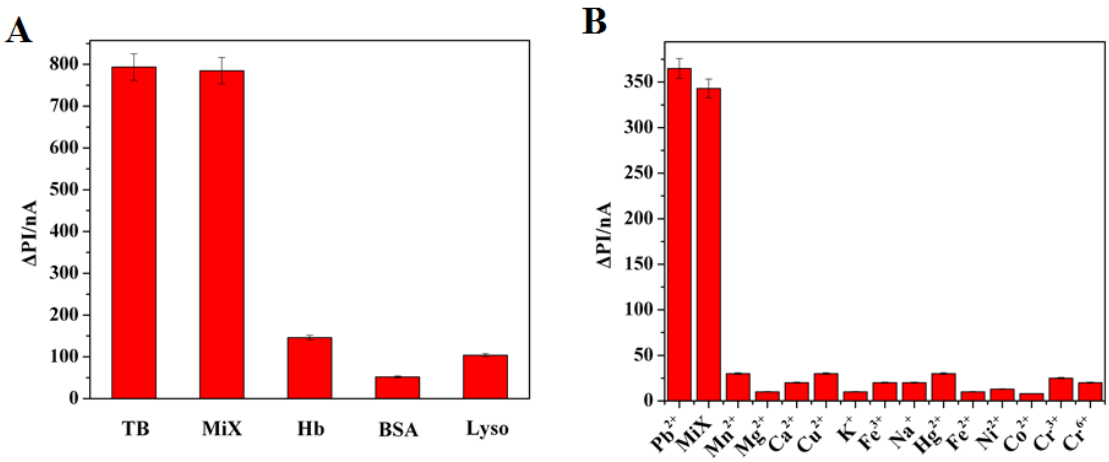

Fig. 6